Ocean Science Journal, Vol. 43 No. 2, 81-90(2008)

Article

Ocean Science Journal

http://osj.kr

A Study of Estuarine Flow using the Roving ADCP Data

KiRyong Kang[1]* and Daniela Di Iorio[2]

[1]*Typoon and Asian Dust Research Laboratory, National Institute of Meteorological Research, Seoul 156-720, Korea*
[2]*Department of Marine Sciences, The University of Georgia, Athens, GA 30602,U.S.A.*

Received 14 January 2008; Revised 10 April 2008; Accepted 27 May 2008

Abstract – A study of estuarine flows during a neap tide was performed using 13-hour roving acoustic Doppler current profiles (ADCP) and conductivity-temperature-depth (CTD) profiles in the Altamaha River estuary, Georgia, U.S.A. The least-squared harmonic analysis method was used to fit the tidal (M_2) component and separate the flow into two components: the tidal and residual (M_2-removed) flows. We applied this method to depth-averaged data. Results show that the M_2 component demonstrates over 95% of the variability of observation data. As the flow was dominated by the M_2 tidal component in a narrow channel, the tidal ellipse distribution was essentially a back-and-forth motion. The amplitude of M_2 velocity component increased slightly from the river mouth (0.45 m/sec) to land (0.6 m/sec) and the phase showed fairly constant values in the center of the channel and rapidly decreasing values near the northern and southern shoaling areas. The residual flow and transport calculated from depth-averaged flow shows temporal variability over the tidal time scale. Strong landward flows appeared during slack waters which may be attributed to increased baroclinic forcing when turbulent mixing decreases.

Key words – estuarine flow, least-squared harmonic analysis, baroclinic forcing, turbulent mixing

1. Introduction

An estuary is a complex system where seawater is diluted with freshwater from land runoff (Dyer 1977). This dilution process takes place because of enhanced turbulence and mixing levels due to many forcing mechanisms like tide-, buoyancy-, wind- and wave-induced motions. In addition, many substances are transported from the estuary to the near-shore zone via advective and dispersive processes. While tidal currents produce large fluxes of material or water, it is the tidally averaged (or removed) residual circulation (or net transport) that controls the net exchange of material. Thus, residual circulation is important for understanding net transport in estuarine systems.

Estuarine circulation results from two important forcing mechanisms: barotropic and baroclinic pressure gradient flows (Jay 1991; Jay and Smith 1990; Simpson 1997). The barotropic pressure gradient flow is driven by horizontal changes in sea surface elevation and is produced by several mechanisms: the propagating tidal wave that changes direction depending on the flooding or ebbing phase of the tide and the amount of freshwater outflow that is directed seaward. The baroclinic pressure gradient is caused by horizontal changes in density and drives the flow towards regions of lower density, which can result in a barotropic response in order to maintain continuity. In general, the barotropic forcing is larger than baroclinic-driven flows. The baroclinic pressure gradient flow is forced by the longitudinal or latitudinal density gradient, with a maximum value at depth and zero at the surface. By averaging over the tidal period or removing the dominant tidal forcing the classical residual circulation is established in the estuary, wherein the landward baroclinic flow at depth is balanced by the seaward barotropic force at the surface.

Many researchers have studied estuarine residual flow. Pritchard (1952, 1956), and Hansen and Rattray (1965) were the first to describe density-driven gravitational circulation in an estuary and Simpson *et al.* (1990) explained the role of horizontal density gradients in creating periodic vertical stratification by straining. Nunes-Vaz *et al.* (1989) studied the role of turbulence in estuarine mass transport

*Corresponding author. E-mail: krkang@kma.go.kr

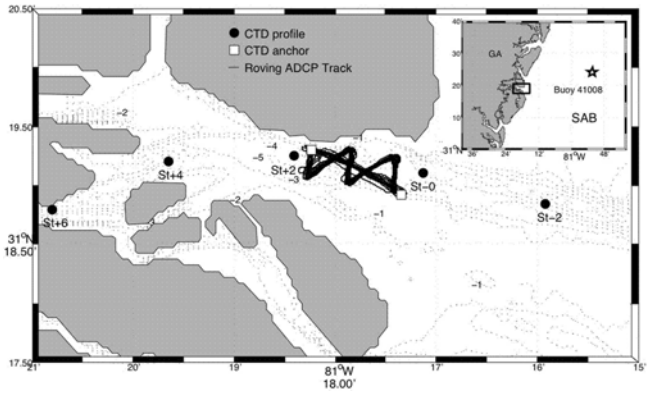

Fig. 1. Study area showing roving ADCP track and CTD casting stations in the Altamaha River Sound. Dotted line indicates the water depth contour in meters.

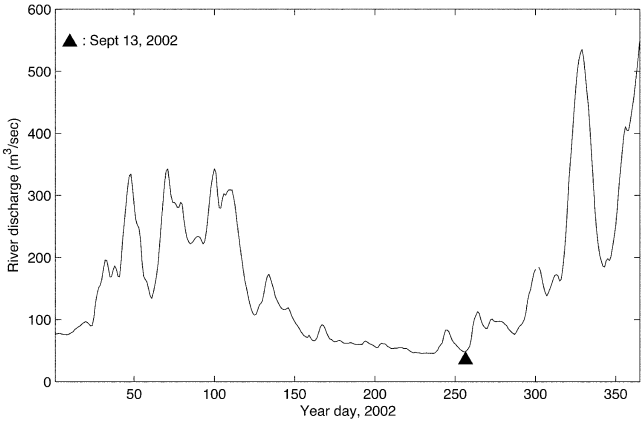

Fig. 2. Time variation of discharge in 2002 showing that our measurement campaign was carried out during a low river transport.

and suggested that the time varying baroclinic-driven flow become maximal during slack water because turbulence and stratification are minimal. Stacey *et al*. (2001) found that the residual flow can be a periodic pulse strongly correlated with the tidal cycle because of the interactions between shear, stratification and mixing.

The estuarine system of the Altamaha River, Georgia, U.S.A., is complex because of the many different pathways that the river can take to the coastal area. Some of the flow is directed southward through the intra-coastal waterway and some northward through various channels (Fig. 1). The Altamaha River is one of Georgia's largest rivers, providing extensive fresh water to coastal sea; river discharge has a large seasonal variability with peak flows during early spring and fall (depending on the number of hurricanes and tropical storm events) and then substantially less during the rest of the year (Fig. 2). The tidal range varies from 1.5 to 3 m during times of strong spring/neap variations. The flow is predominantly ebb-dominated, with magnitude >1 m/sec in the Altamaha Sound, where the width of main channel is about 1 km with a maximum depth of 8-10 m (Kang and Di Iorio 2006).

This study is focused on two things: one is to see how the estuarine flow pattern changes with time after removing the dominant tidal component and then check if there is a relation with baroclinic force-driven flow in the Altamaha River estuary during the period when the total river discharge was very low. Another is to introduce a method to analyze the current measurement data, especially that obtained from the roving ADCP. The design and data processing procedure is described in Section 2, and in Section 3 we discuss the characteristics of the surface density distribution, the latitudinal and longitudinal density variations as a function of depth, the semidiurnal lunar tide (M_2) characteristics, residual flow, and transport. Section 4 summarizes significant findings.

2. Field sampling and data processing

During the September 2002 LTER (Long Term Ecological Research) quarterly monitoring survey, a 13-hour time series of roving acoustic Doppler current profiles (ADCP) and conductivity-temperature-depth (CTD) profiles were performed at neap tide to investigate the cross- and along-channel variations of the current structure in the Altamaha River Sound. This field campaign was specifically designed to resolve the residual flow and hence the net transport across three sections in the main channel by estimating the M_2 component using the least-squared sense. Residual flow in this context refers to the flows without the principal lunar semidiurnal tide (M_2 component). Figure 1 shows the study area with the ship track (solid line) and CTD profile stations. Blanked squares indicate CTD profiles over the 13-hour time series sampled on Sept 13, 2002 (neap tide) and open circles show the CTD transect locations carried out on Sept 18, 2002. During the 13-hour experimental period, ocean winds, measured 30 km offshore, blew from the southerly to northeasterly direction with magnitudes 2-7 m/sec (not shown here). The river discharge gauged at Doctortown, about 95 km upstream in the Altamaha River, was about 50 m^3/sec (~2.5% of sectional transport in the

river mouth); that is, almost minimum value of year (Fig. 2). Since the wind direction varied with anticlockwise tendencies, sea surface status was relatively calm, and river discharge was not large enough to affect the vertical stratification; we assumed that these atmospheric factors can be ignored in the estuarine flow formation during this study period.

In this study, a 1200 kHz broadband ADCP from RD Instruments mounted to a mast on the port side was used, together with flow through thermosalinographs and an SBE25 CTD profiler from SeaBird. The ADCP data were sampled at 2 Hz continuously for 13 hours with 0.25 m vertical bin size. The ADCP was operated in bottom tracking mode with the ship's gyrocompass as an external heading. The ship track line was in a zigzag shape specifically designed to obtain three cross sections along the channel. Each zigzag took approximately 45 min and a total of 17 such transects were made over the course of the 13 hour-tidal cycle. For each cross section we constructed a grid having a resolution of 30.8 m in the latitudinal direction and a varying resolution in the horizontal in order to encompass the horizontal spread of the transect lines (Fig. 3). The distance between section A and C was about 1.43 km, and the horizontal resolution for section A, B and C was 291, 264 and 238 m, respectively. The mean position of all samples in each grid box was shown in Figure 3 as open circles. These points represent the grid position of the flow and surface salinity observation. Each profile of current within the grid represents an approximate average over 20 seconds (while the ship was within each grid) and 17 such averaged profiles exist at each grid point corresponding to 13 hours of data.

As the data for each grid were unevenly sampled in time, the velocity profiles and depth time series were linearly interpolated at 30 min intervals prior to the tidal analysis. To

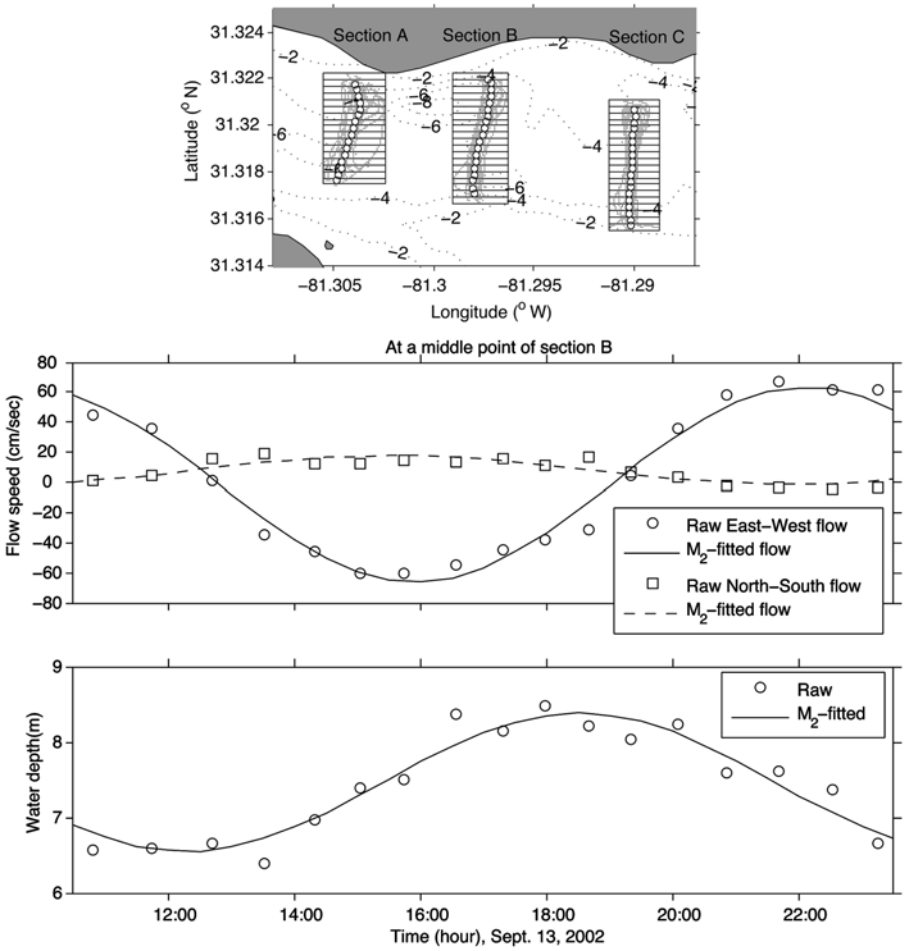

Fig. 3. Roving ADCP tracks and averaged location of 1-second (about 30 m) grid cell in North-South direction. The circles indicate the mean location of each grid and solid lines show the tracks of the ship. The dotted line indicates the depth contour in meter unit. The lower panels show an example of M_2 tidal constituent fit to the depth-averaged velocity and pressure data.

capture the tidal flow characteristics, we applied the tidal harmonic analysis method developed by Foreman (1996) and implemented into MATLAB as T_TIDE by Pawlowicz (2002) to depth-averaged flow data,

$$\overline{U}(x_i, y_j, t) = \frac{1}{\overline{h}(x_i, y_j)} \int_0^h U(x_i, y_j, z_k, t) dz \quad (1)$$

And mean water depth $\overline{h}(x_i, y_j)$ was the measured value at each grid cell. The velocity vector $U = (u, v)$ is the east-west and north-south velocity component, x_i is the along channel coordinate with i=1,2,3 representing the number of grids along the channel (section A, B, and C respectively), y_j is the cross channel coordinate with j=1,...,M is the cross channel grid number going from south to north, z_k is the depth with k=1,2,...,N is the vertical bin number going from just below the surface (z_1=-z_b, where z_b is the blanking distance of the ADCP) to the bottom, and t is the time step. We have not corrected for variable surface elevation due to the tidal oscillation as described by Li *et al*. (2004) since most of our measurements are based on depth-averaged results. The lower panel of Figure 3 shows an example of the depth-averaged flow and the water depth with the M_2 tidal constituent superimposed. This example represents the flow in the middle of section B at coordinate (x_2, y_{10}).

Both the east-west (solid curve) and the north-south (dashed curve) flow are plotted together with a least squares fit of the M_2 tide showing a strong correlation with the observed data. The tidal height also shows a good fit in a least squares sense (minimum difference between observed and fitted values) indicating that this area is dominated by the semi-diurnal lunar tide. The great variability in the water depth measurement may correspond to bathymetric features within the grid influencing the measurement rather than the tidal height. Table 1 lists the amplitude and phase parameters for this fit. The semidiurnal M_2 component explained over 95% (maximum 97%) of the total variance of the depth-averaged flow and 94% of the tidal height variance. This method of applying an M_2 tide to roving ADCP data was used by Li *et al*. (2000) and Li *et al*. (1998) for inferring the tidal elevation in shallow waters and for separating barotropic and baroclinic flows. In the Altamaha estuary case, the phase difference between the velocity and water depth fits was approximately -75.5 degree indicating that the M_2 tidal propagation in this area is between a progressive and a standing wave.

The depth-averaged residual flow was estimated by subtracting the M_2 component derived from the depth-averaged flow,

$$\overline{U}_r(x_i, y_j, t) = \overline{U}(x_i, y_j, t) - \overline{U}_{M2}(x_i, y_j, t) \quad (2)$$

where bar corresponds to depth averaged values and $U_{M2} = (u_{M2}, v_{M2})$ is the M_2 tidal flow constituent using depth averaged flow and at each depth. The residual volume transport within each grid cell was then calculated by,

$$Q(x_i, y_j, t) = h(x_i, y_j, t) \Delta y \overline{U}_r(x_i, y_j, t) \quad (3)$$

where Δy is the latitudinal grid size of 30.8 m and h is the time varying water depth.

3. Results

Density distribution

One key feature in most estuaries is the longitudinal salinity distribution ranging from freshwater to seawater, which is a driving mechanism for the baroclinic or gravitational circulation. A 'sideways' estuarine circulation can exist for wide estuaries having lateral density gradients and for relatively narrow estuaries where frictional effects are important (Valle-Levinson *et al*. 2003). As the flow strains the horizontal gradient, periodic stratification will exist. Figure 4 shows density profiles taken during the low and high water transects along the channel between stations -2 and 6 km in the Altamaha. The profiles show that the estuary is essentially well-mixed in vertical during this time with weak stratification existing between 0 and 2 km (where the roving ADCP surveys took place). The tidal excursion distance based on these salinity profiles is approximately 8 km. Typically the longitudinal density

Table 1. An example of the amplitude (*Maj*or and *Min*or axes) and phase (Pha) for the M_2 tidal constituent fit to the velocity and sea level height. 95% confidence intervals are shown by the error terms (eMaj, eMin and ePha).

	Maj (m/sec, m)	eMaj (m/sec, m)	Min (m/sec)	eMin (m/sec)	Pha (deg)	ePha (deg)
Velocity	0.660	0.091	0.016	0.052	315.29	7.95
Sea level	0.93	0.17			30.85	10.83

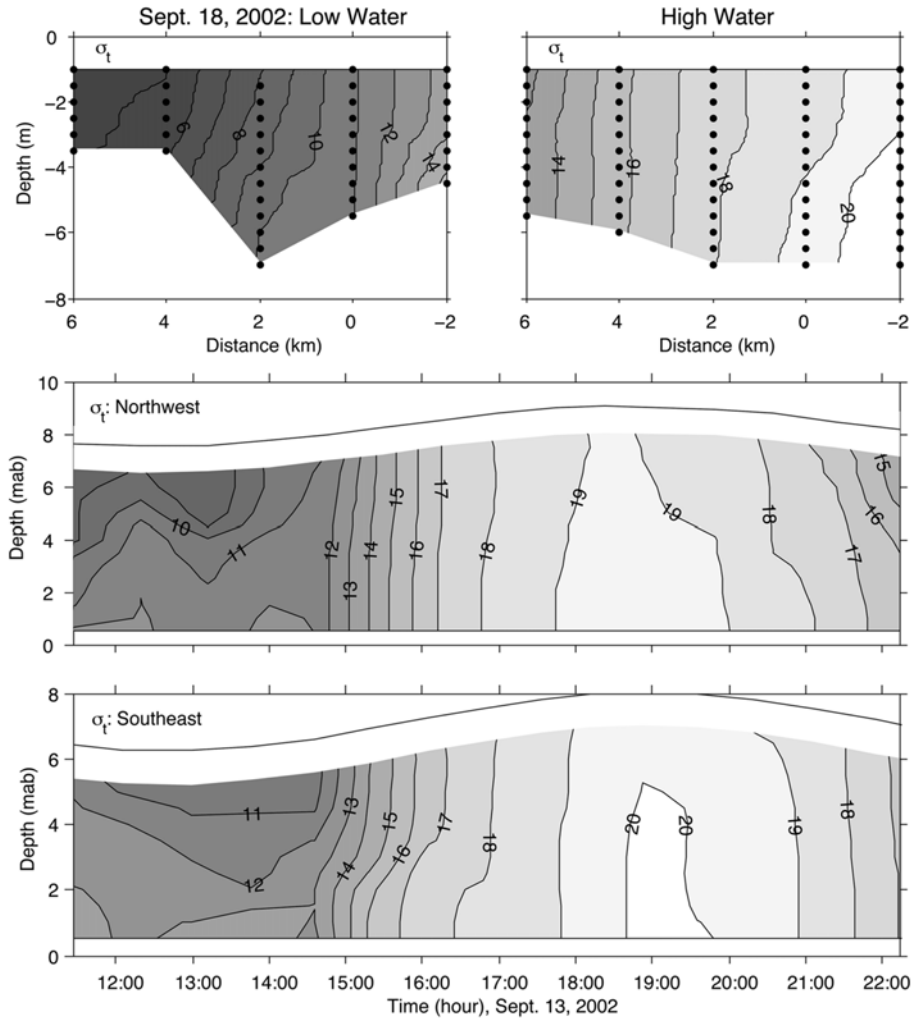

Fig. 4. Density distribution along the CTD transection and time series at the two anchor stations. Depth unit 'mab' means meters above bottom.

gradient has been measured in past observations with similar river transport to be 1.2×10^{-3} kg/m^2 and can play a strong role in the tidal straining process.

Time series of the vertical density profiles for the northwest and southeast stations are also shown in Figure 3. The time difference between each profile is approximately 40 min, which was the traveling time for the distance 1.4 km between two stations. Both stations show more stratification during slack low water, which is then quickly mixed away at the onset of the flooding tide, becoming relatively homogeneous at high water. This is consistent with the strain induced periodic stratification (SIPS) process described by Simpson *et al*. (1990). The largest difference between these two stations is the greater amount of fresher water that exists at the northwest station during the ebb to low water tidal cycle. The northern side of the channel is deeper than the southern side, which may be the result of scouring from the intra-coastal waterway (Fig. 1) and this channel may contribute to the amount of freshwater on this side during the ebbing tide.

Surface density distributions interpolated over the zigzag grid are shown in Figure 5 for different times in the tidal cycle. Each panel corresponds to approximately 40 min of time and so some tidal aliasing is incorporated into the data. The most striking feature evident is the latitudinal density gradient that exists during flood and ebb tide. During the flood tide, the water in the center of the channel has a higher density than along the coastal boundaries, indicating that a residual flow outward may occur along the shoaling areas of the channel. For the ebb tide, the density distribution

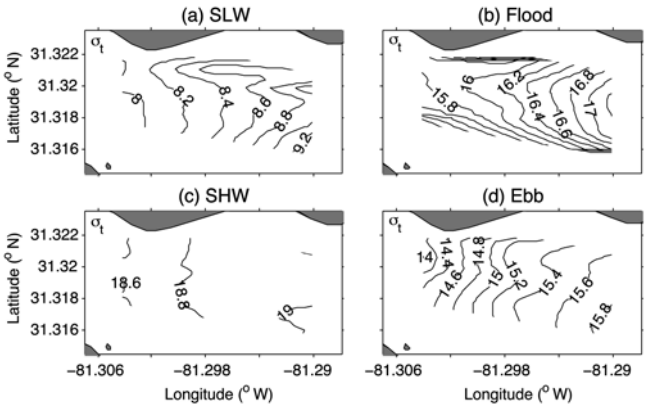

Fig. 5. Horizontal distribution of surface water density with tidal period. SLW: Slack Low Water, SHW: Slack High Water.

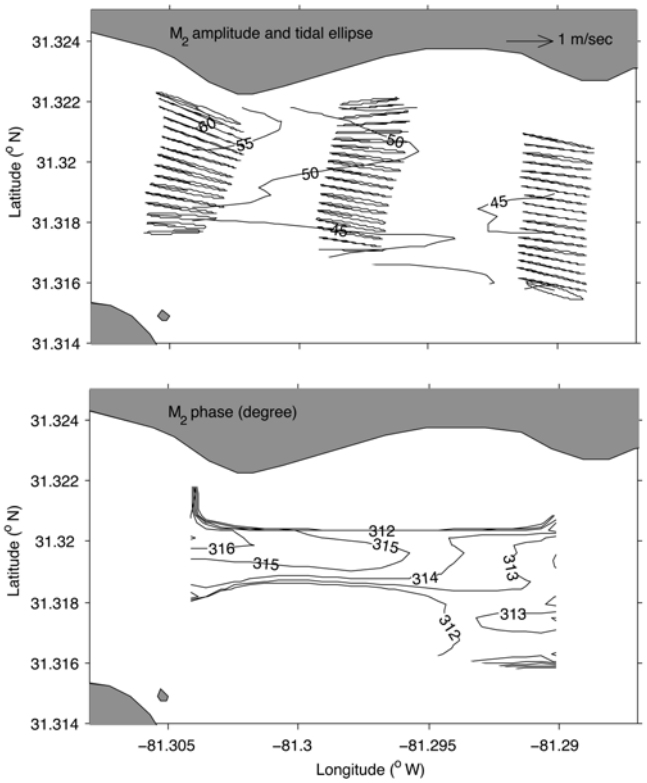

Fig. 6. Tidal ellipse, amplitude and phase distribution of the M_2 component. The phase is the degrees relative to Greenwich time.

shows a higher density along the southern coastal boundary than along the northern boundary; this is consistent with the CTD profiles in Figure 4. The latitudinal density difference at the surface is approximately 0.6 kg/m^3 for flood and ~0.4 kg/m^3 for ebb. The CTD profiles also show a greater lateral density gradient occurred at depth in the northwest as compared to the southeast stations. During slack low water some surface latitudinal variations exist, indicating higher saline water stored over the shoaling area to the north. At the end of flood tide practically no latitudinal variations exist.

Tidal flow

Tidal flow plays a significant role in the dynamics of estuaries. The characteristics of tidal motion are strongly dependent on the shape of the estuary itself, in particular its width, length, and bottom topography. Since estuarine environments are generally shallow compared to the tidal wave length, bottom friction can alter the tidal motion. Tidal energy is dissipated due to friction between the mean flow and seabed. This frictional damping is a non-linear process that depends on the square of the current speed and inversely on the depth. If there is a large amount of tidal energy dissipation, then the tidal wave becomes progressive and the amplitude and current may not be 90 degrees out of phase. In some extreme cases the maximum flood currents take place at high water, which also coincides with maximum salinity (Dyer 1997). In the Altamaha River high tide occurs later for points further into the estuary and therefore can be described as a progressive wave over the whole estuarine domain.

Figure 6 shows the characteristics of the amplitude and phase of the semidiurnal lunar tidal component (M_2, T=12.42 hours) as a function of space over the transect domain. As only 13 hours data were collected the M_2 component was solely included in the analysis. The tidal ellipse shows that the flow pattern in the estuary is predominantly horizontal and somewhat aligned with the coastal boundaries. Maximum flows are predominantly in the northwest area as shown by the elongated ellipses. From the southeastern sampling region toward the northwest, the amplitude is increased from 45 cm/sec to 60 cm/sec, presumably due to changes in the water depth. The tidal phase over this short longitudinal section shows little variation except for the shoaling regions in both the north and south where the phase is significantly altered, presumably due to increased bottom friction.

Horizontal distributions of the surface, bottom and depth-averaged flows together with the M_2 tidal constituent from depth-averaged data are shown in Figure 7. The surface flood flow shows slightly greater speeds in the center of the channel whereas the ebb flow is more concentrated on the northern shore. The near bottom flows are greatly reduced because of bottom friction, and show more lateral variability

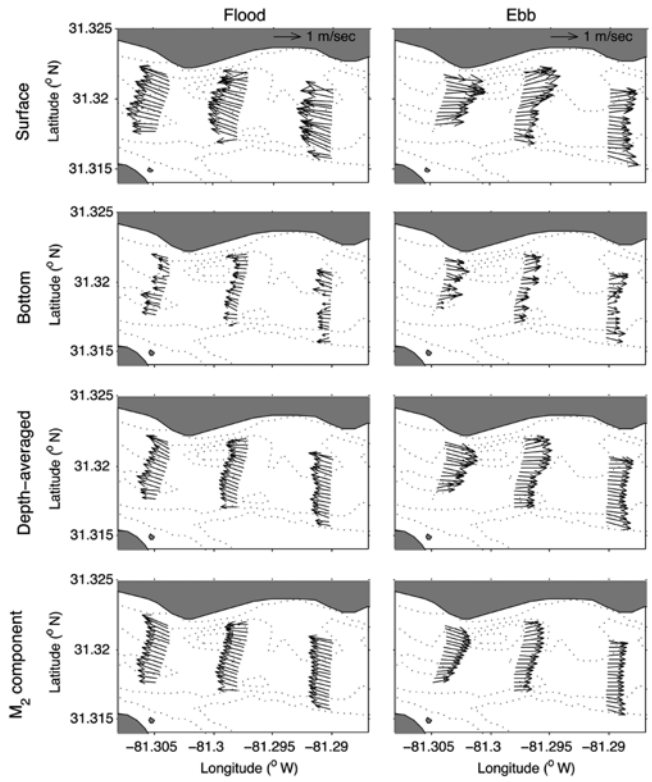

Fig. 7. Horizontal flow distribution at the surface, bottom, depth-averaged and M_2 component during the flood and ebb tides. The surface layer indicates the first bin of the ADCP that is about 2 m below the surface, and bottom is taken from the last bin of ADCP data.

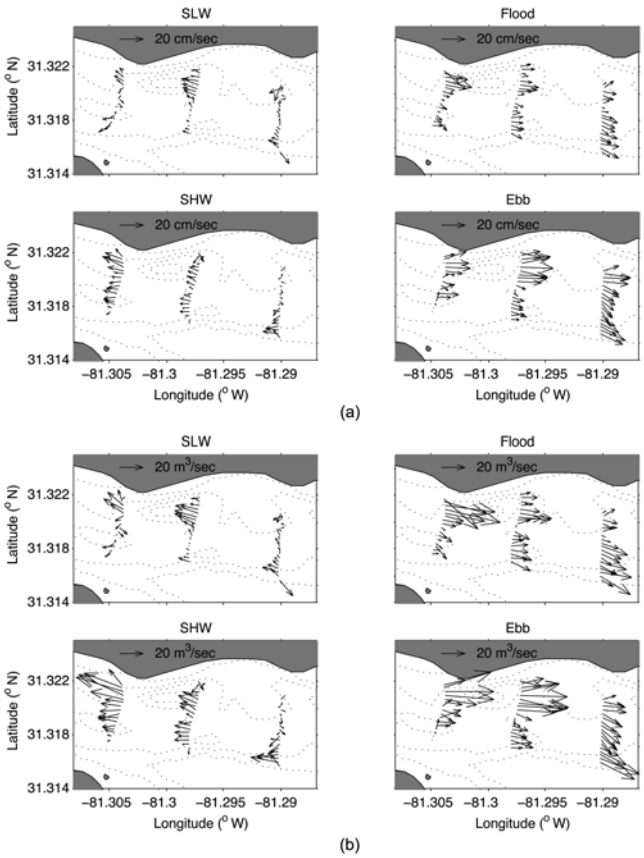

Fig. 8. Horizontal distribution of (a) the residual (M_2-removed) flow from the depth-averaged current and (b) its net transport.

on ebb than on flood. The depth-averaged flow shows ebb-dominant flow (as the magnitudes are greater on ebb than on flood). This is caused by either the net river discharge or the nonlinear interaction of the M_2 tide with bottom friction creating and M_4 tidal harmonic that has twice the period of the M_2 tide (Blanton *et al*. 2002). M_2 component, which represents a best fit to the time varying depth-averaged flow, smoothes out the lateral and longitudinal variations. M_2 flood is slightly greater than the depth-averaged flow, resulting in a positive (seaward) residual flow as will be shown. In contrast, the depth-averaged ebb flow is greater than the M_2 component.

Depth-averaged, residual flow and transport

The depth-averaged residual flow, $\overline{U}_r(x_i, y_j, t)$, calculated from the equation 2 is shown in Figure 8 over four stages of the tidal cycle. The most interesting thing to note is the residual seaward flow for both the flood and ebb tides and weaker landward flow during slack water. Generally speaking, the baroclinic flow is driven by the pressure gradient due to the longitudinal density gradient and traditionally it has been considered constant over tidal time scales. Recently Stacey *et al*. (2001) showed that the velocity scale for the baroclinic flow (modified here to include the density gradient rather than the salinity gradient) could be written as,

$$u_g = \frac{\frac{1}{\rho}\frac{\partial \rho}{\partial x} g H^2}{u_*} \tag{4}$$

where H is a depth scaling and u_* is the friction velocity representing the turbulence levels and hence mixing. As the friction velocity increases, mixing increases and therefore the baroclinic flow decreases; as mixing decreases during slack water due to low flows and more stratified conditions the baroclinic flow increases. This scaling result is consistent with the results of Nunes-Vaz *et al*. (1989), who demonstrated that the baroclinic mass flux is greatest during

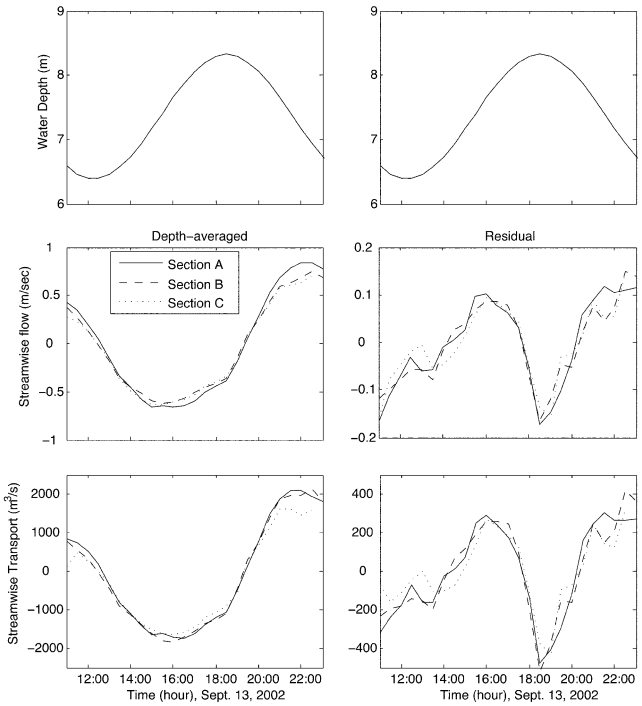

Fig. 9. Time variations of the depth-averaged and residual flow and total net transport of each section.

the strongest stratification period, which is at a time of minimum turbulent kinetic energy. They further showed that the baroclinic-driven flow has a temporal variation that is consistent with the variations of turbulent mixing, which are at the tidal (M_4 period) and spring-neap time scales.

In order to estimate the scale of baroclinic-driven velocity, both horizontal density gradient and frictional velocity are obtained at the same time. However, since the turbulent-related properties were not observed during this study period, we used the Reynold's stress value obtained on May 31, 2005 (Fig. 9 of Di Iorio and Kang 2007) to estimate the friction velocity. The data of May 31, 2005, were also obtained during the neap tide and small river discharge period (< 100 m^3/sec). Table 2 showed an example of velocity scale of baroclinic-driven flow in the Altamaha River Estuary. Horizontal density gradient showed peaks for High Water (HW) and Low Water (LW) and friction velocity showed one order difference between HW (or LW) and the flood (or ebb) tide. This condition makes minimum value (~0.67 cm/sec) for flood and ebb, and maximum (16~24 cm/sec) for HW and LW in the baroclinic-driven velocity scale.

Assuming that the estuarine flow system be controlled by tide and horizontal density gradient based on atmospheric

Table 2. An example of the velocity scale for the baroclinic flow in the Altamah River estuary. Density gradient values based on the observation of Sept., 2006, and the friction velocity obtained on May 31, 2005, were used.

	High and Low Water	Flood and Ebb
$\frac{1}{\rho}\frac{\partial \rho}{\partial x}gH^2$ [cm^2/sec^2]	4~6	0.0~0.2
U_* [cm/sec]	0.25	3.0
U_g [cm/sec]	16~24	0.0~0.67

effects such as wind and freshwater discharge are ignorable, the simplified momentum equation describing the barotropic flow is,

$$\frac{\partial U}{\partial t} = -\frac{1}{\rho}\frac{\partial p}{\partial x} + \frac{\partial}{\partial x}\left(\nu_t \frac{\partial U}{\partial z}\right) \quad (5)$$

where the Reynolds stresses have been parameterized in terms of the vertical mixing of momentum and shear. In general, during the ebb tide, when mixing is weak, ν_t is small as a result of increased stratification; more shear thus develops, causing increased acceleration of the surface waters. On flood, as the stratification is destabilized, ν_t is large and so higher momentum surface waters are mixed down to the bottom thus increasing the near bed flow. Both the baroclinic and barotropic mechanism described create temporally varying residual flows that are dependent on the turbulence-enhanced mixing asymmetries and are thus not easily separated.

Figure 8a also shows some latitudinal variation of the residual flow. Maximum flows of 0.2 m/sec occurred along the northern side of the channel for sections A and B and on the southern side at section C. This is more apparent in Figure 8b where the residual volume transport, estimated using equation (3), is shown. The transport is more enhanced where the depths are greatest. During the slack water, the data shows that a significant amount of transport is upstream which has implications for moving particulates and biological organisms from the coastal ocean into the estuarine environment.

The time variability of the residual flow and transports is shown in Figure 9 over the tidal cycle sampled. The total transport shows that the tides move a significant amount of water into and out of the estuary. For each of the sections, the streamwise transports are not different, having the same phase and similar magnitudes (ranging from -1800 m^3/sec to a maximum of 2000 m^3/sec on ebb). The depth-averaged flow speed corresponds to -0.6–0.8 m/sec. The residual

volume transport shows positive (seaward) values during the flooding and ebbing tide and negative (landward) values during slack waters. Maximum speed of the residual flow (M_2-removed) was almost close to 20 cm/sec. Comparing the velocity scale and time variation pattern of baroclinic-driven flow in Table 2, this residual flow speed and variation pattern matches very well. This temporal variability is consistent within all cross sections and not constant over the tidal time period. It should be noted that these measurements were carried out during a neap tide when presumably mixing activity was weak; we could expect the residual flow to be maximal at this time. Comparison with a spring tide case is also essential in the future.

4. Concluding Remarks

The estuarine flow and its water volume transport in the Altamaha River Estuary, GA, were described based on a 13-hour roving ADCP and CTD profile data set. The harmonic analysis method was used to separate the tidal and residual components from the depth-averaged flow data. Net transport by the residual flow was also estimated to see changes on the circulation pattern over the tidal cycle. The semidiurnal component (M_2) was well fitted into the depth-averaged current data, covering over 95% of variance of the flow data. Tidal amplitude and phase and time variation of residual flow were presented for introducing the characteristics of estuarine flow pattern. The water volume transported by the residual flow showed that the residual circulation is a result of barotropic- and baroclinic-driven flow and has also a tide-like periodic character.

The spatial density gradient is a main source of the baroclinic force-driven flow, especially when the tide-driven barotropic effect was minimal. In the area of 7-8 km from the river mouth, the longitudinal density gradient for slack low and high waters become maximal. In the local viewpoint the density gradients were 1.33 and 0.67 kg/m^3/km for the slack low water (SLW) and slack high water (SHW), respectively; however, when the area was extended including the tidal excursion distance, these gradients changed to 0.83 and 1.08 kg/m^3/km. At the river mouth area, density (σ_t) ranged from 11 to 20. It should also be noted that the density distribution along the channel was compressed from the flood tide to slack high water, while it became loose from the ebb to slack low water. So, without other external forcing, i.e. wind or river discharge, the baroclinic force could become a dominant factor in controlling flow in the estuary since tide-driven barotropic forcing at the end of both flood and ebb tides is minimum and enhance turbulent kinetic energy becomes almost zero.

According to the tidal ellipse distribution for M_2 component, the flow shows back-and-forth type of motion. The length of major axis of the ellipse varied 0.6–0.90 m/sec and minor 0.08–0.12 m/sec. The amplitude of the M_2 component was increased a little, ranging from 0.45 to 0.6 m/sec to landward, and most of the area was in-phase, with the exception of the northern part of section B. The flow pattern also showed stronger flow in the deeper area. Even the residual flow of the ebb case was stronger than the flood case. Both flood and ebb tides showed seaward residual flow with a maximum magnitude of 0.2 m/sec. The results of comparison between this residual flow and the velocity scale of baroclinic-driven flow using the equation (2) indicated that the residual flow could be driven by the baroclinic force especially during the SHW and SLW. The velocity scale of baroclinic-driven flow for the SHW and SLW was 0.16-0.24 m/sec and the friction velocity as an index of turbulent mixing showed one order of difference between the slack waters and the flood (or ebb). Because the barotropic forcing by tide became almost zero for the slack waters, the only factor driving the estuarine flow system remains the high baroclinic effect and low turbulent mixing between ocean and river channel when the other factors like wind stress or river discharge are ignorable.

The volume transport by the residual flow showed landward movement for the both slack waters with maximum 42.48 m^3/sec, and seaward for the flood and ebb tides with maximum 48 m^3/sec. The northern part of the channel especially demonstrated a lager amount of transport because of the bottom topography. Since the baroclinic term is increased as depth increases, so the deeper the water depth, the stronger the baroclinic force. The time variation of the streamwise residual transport showed an interesting fact: the residual transport for the slack water has negative peak values in all sections, and for the flood and ebb tides, the streamwise residual transport has positive values. Finally, it should also be noted that due to the lack of sufficient observation data we used only a single tidal component for calculating the residual (M_2-removed) flow. But it is possible to include more tidal components rather than one. This limitation can be overcome by performing long-term observation, which will be a part of future studies.

Acknowledgments

This work was supported by the NSF (OCE-9982133) as part of the Georgia Coastal Ecosystems Long Term Ecological Research (GCE-LTER) project (http://gce-lter.marsci.uga.edu/lter/index.htm) and by the University of Georgia Research Foundation, Faculty Research Grant program. The authors would like to thank Captain Raymond Sweatte and the crew of the R/V Savannah for their support in towing ADCP and CTD profiling. The authors express their gratitude to two reviewers for their valuable comments which helped to clarify our objectives and to verify the baroclinic force-driven velocity scale.

References

Blanton, J.O., G. Lin, and S.A. Elston. 2002. Tidal current asymmetry in shallow estuaries and tidal creeks. *Cont. Shelf Res.*, **22**, 1731-1743.

Di Iorio, D and K. Kang. 2003. Some Physical factors that affect turbulent mixing in Altamaha Sound, Georgia. p. 735-738. In: *Proceedings of the 2003 Georgia Water Resources Conferences*, April 23-24, 2003, ed. by K. J. Hatcher. The University of Georgia, Athens, GA.

Di Iorio, D. and K. Kang. 2007. Variations of turbulent flow with river discharge in the Altamha River Estuary, Georgia. *J. Geophy. Res.*, **112**, C05016.

Dyer, K.R. 1997. Estuaries: A Physical Introduction. John Wiley and Sons. 197 p.

Dyer, K.R. 1982. Mixing caused by lateral intense seiching within a partially mixed estuary. *Estuar. Coast. Shelf Sci.*, **15**, 443-457.

Foreman, M.G.G. 1979-1996. Manual for Tidal Currents Analysis and Prediction. Institute of Ocean Sciences, Patricia Bay Sidney, British Columbia.

Hansen. D.V. and M. Rattray. 1965. Gravitational circulation in straits and estuaries. *J. Mar. Res.*, **23**, 104-122.

Ianniello, J.P. 1977. Tidally induced residual currents in estuaries of constant breadth and depth. *J. Mar. Res.*, **35**, 755-786.

Jay, D.A. 1991. Estuarine salt conservation: A lagrangian approach. Estuar. *Coast. Shelf Sci.*, **32**, 547-565.

Jay, D.A. and J.D. Smith. 1990. Circulation, density structure and neap-spring transitions in the Columbia River estuary. *Prog. Oceanogr.*, **25**, 81-112.

Kang, K. and D. Di Iorio. 2006. Depth- and current-induced effects on wave propagation into the Altamaha River Estuary, Georgia. *Estuar. Coast. Shelf Sci.*, **66**, 395-408.

Li, C. and A Valle-Levinson. 1998. Separating baroclinic flow from tidally induced flow in estuaries. *J. Geophy. Res.*, **103**, 10405-10417.

Li, C., A. Valle-Levinson, L.P. Atkinson, and T.C. Royer. 2000. Inference of tidal elevation in shallow water using a vessel-towed acoustic Doppler current profiler. *J. Geophy. Res.*, **105**, 26225-26236.

Li, C., J. Blanton, and C. Chen. 2004. Mapping of tide and tidal flow fields along a tidal channel with vessel-based observation. *J. Geophy. Res.*, **109**, C04002.

Li, C. and J. O'Donnel. 1997. Tidally driven residual circulation in shallow estuarine with lateral depth variation. *J. Geophy. Res.*, **102**, 27915-27929.

Nunes-Vaz, R.A., G.W. Lennon, J.R. de Silva Samarasinghe. 1989. The negative role of turbulence in estuarine mass transport. *Estuar. Coast. Shelf Sci.*, **28**, 361-377.

Pawlowicz, R., B. Beardsley, and S. Lentz. 2002. Classical tidal harmonic analysis including error estimates in MATLAB using T_TIDE. *Computers and Geosci.*, **28**, 929-937.

Pritchard, D.W. 1952. Salinity distribution and circulation in the Chesapeake estuarine system. *J. Mar. Res.*, **11**, 106-123.

Pritchard, D.W. 1956. The dynamic structure of a coastal plain estuary. *J. Mar. Res.*, **15**, 33-42.

Simpson, J.H. 1997. Physical processes in the ROFI regime. *J. Mar. Syst.*, **12**, 3-15.

Simpson, J., H. Burchard, N.R. Fisher, and T.P. Rippeth. 2002. The semi-diurnal cycle of dissipation in a ROFI: Model-measurement comparisons. *Cont. Shelf Res.*, **22**, 1615-1628.

Simpson, J.H., J. Brown, J. Matthews, and G. Allen. 1990. Tidal straining, density currents, and stirring in the control of estuarine stratification. *Estuaries*, **13**, 125-132.

Stacey, M.T., J.R. Burau, and S.G. Monismith. 2001. Creation of residual flows in a partially stratified estuary. *J. Geophy. Res.*, **106**, 17013-17037.

Valle-Levinson, A., C. Reyes, and R. Sanay. 2003. Effects of bathymetry, friction, and rotation on estuary-ocean exchange. *J. Phys. Oceanogr.*, **33**, 2375-2393.